RESEARCH ARTICLE | MARCH 20 2026

Correlation functions in heterodyne optical fiber dynamic light scattering: A laser velocimetry method for tracking active matter at the nanoscale

Anastasia Christoulaki ; Eric Buhler

J. Chem. Phys. 164, 114202 (2026)
https://doi.org/10.1063/5.0303786

The Journal of Chemical Physics ARTICLE pubs.aip.org/aip/jcp

Correlation functions in heterodyne optical fiber dynamic light scattering: A laser velocimetry method for tracking active matter at the nanoscale

Cite as: J. Chem. Phys. 164, 114202 (2026); doi: 10.1063/5.0303786
Submitted: 24 September 2025 • Accepted: 2 March 2026 •
Published Online: 20 March 2026

Anastasia Christoulaki and Eric Buhler[a)]

AFFILIATIONS

Université Paris Cité, Matière et Systèmes Complexes, UMR CNRS 7057, Physics Department, Bâtiment Condorcet, F-75013 Paris, France

[a)]Author to whom correspondence should be addressed: eric.buhler@u-paris.fr

ABSTRACT

Heterodyne dynamic light scattering is a powerful interferometer allowing determination of velocities and directions of nano-sized objects that are too small to be tracked using conventional optical microscopy. Here, their scattered signal is directly mixed in optical fibers with that of a local oscillator (LO) originating from the same laser source, thus offering easy and precise control of the LO reference signal and high detection sensitivity over the entire range of scattering vectors. In this paper, we detail the expression of the heterodyne intensity correlation functions, which depend both on the modulation produced by the particle scattering processes but also on the phase shift introduced by the difference in optical path taken by the two interfering fields in the fiber. We subsequently study various situations ranging from pure Brownian diffusion to ballistic motion. In particular, we detail the analysis of the motion of photocatalytic active nanoparticles capable of autonomous propulsion when exposed to UV irradiation. In such a case, the heterodyne intensity–intensity correlation function is an oscillating function of the lag time with a velocity-dependent frequency allowing both speed and propulsion direction of active nanoparticles to be accurately determined.

I. INTRODUCTION

Heterodyne detection originally developed for the detection of radio waves and microwaves is widely used in various fields currently, ranging from quantum devices and optics to gravitational wave search.[1,2] This technique plays a major role in the detection of nuclear magnetic resonance and scanning tunneling spectroscopy, but it has also been used in atomic force microscopy.[3] Heterodyne optical detection involves an optical signal that is mixed at the detector with waves from a local oscillator (LO) and allows very high frequencies to be determined. On this same principle, heterodyne photon correlation laser spectroscopy makes it possible to measure the speeds of molecules or nano-sized particles and thus constitutes an interferometric technique of choice for nano-objects (<100 nm) that are too small to be able to be followed by conventional optical microscopy techniques. Conducting this type of experiment is difficult and delicate using conventional optical components and mounts, but the use of optical fibers has greatly simplified its implementation.[4–7]

Above all, it is necessary to clarify the vocabulary associated currently with heterodyne and homodyne detections in light scattering. While in the light wave communication and radar literature the term homodyne is used when the signal is mixed with a non-frequency-shifted reference signal (local oscillator) before the detector, a different convention is used in the dynamic light scattering (DLS)—or photon correlation spectroscopy—literature: in the *homodyne* DLS (or self-beat) method, only the light scattered from the sample is detected, while in the *heterodyne* DLS method, the signal of the LO, which usually is a small fraction of the intensity of the incident laser light, is mixed with the scattered light on the detector[8–12] (we should note a different use of these terms in some earlier spectroscopic light-beating literature). If the reference signal is shifted relative to the incident laser wavelength, we speak of super

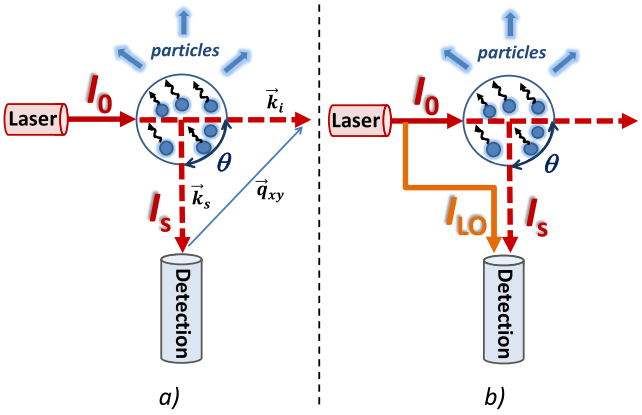

FIG. 1. Comparison of *homodyne* (self-beating) (a) and *heterodyne* (mixing) (b) configurations used for DLS. I_{LO} represents the reference beam (local oscillator), whereas I_0 and I_s represent the incident laser intensity and scattered intensity from the sample, respectively. Incident ($\vec{k_i}$), scattered ($\vec{k_s}$), and scattering ($\vec{q_{xy}}$) wave vectors are drawn in Fig. 1(a).

heterodyne DLS. Figure 1 illustrates the two measurement configurations. In such *heterodyne* DLS experiments, the reference beam can be obtained either by deflecting a small fraction of the intensity of the laser light before it reaches the sample, as in the present case, or by scattering part of the incident light from the wall of the sample tube or a solid object immersed in the scattering volume, e.g., a needle.[13–19] In either case, the reference beam, I_{LO}, is mixed with the light scattered from the sample, I_s, on the detector.

If nano-objects undergo both directed motion (due to an electric, magnetic, thermal, or gravitational field, or even autonomous directed propulsion) and random diffusion, equations for forced diffusion can be used to describe this situation. Although DLS is a well-established technique for measuring particle size in the range of a few nanometers to a few micrometers and a technique of choice for studying the dynamics of solutions, and in particular diffusive processes due to Brownian motion, it does not allow access to the average velocity of particles. The study of directed motions or forced diffusion requires advanced heterodyne DLS (HDLS) experiments,[20–22] allowing measurement of dynamical structure factors characterized by both diffusive (stochastic) and ballistic (directional) processes.

Heterodyne DLS is thus an interferometric technique of choice for measuring the speed of molecules or nano-objects that are too small to be followed by microscopy. Conducting such an experiment, however, proves to be very tricky, especially when using conventional optical components and mounts, which explains the limited number of reported attempts. Some important applications of this "laser velocimetry" method were made in the 1970s to probe blood flow in vessels,[13,14] flowing solution of macromolecules, or in electrophoresis where an electric field is applied.[15] In most studies, the reference signal was obtained by scattering part of the incident light using a scratch or reflection on the wall of the sample tube or a solid object present in the scattering volume, for example, a needle.[13–19] Such methods introduce numerous arbitrary light reflections that are difficult to control and assess, which limits and makes it difficult to vary the scattering angle (equivalently the scattering vector). A wide angular variation is, however, essential for accurately determining the direction of propulsion of a particle. Furthermore, the intensity of the local oscillator signal is arbitrary and uncontrolled even though it constitutes a crucial experimental parameter, which must be chosen and dosed according to the study systems. These technical difficulties certainly explain the lack of subsequent HDLS studies. It is only much more recently that DLS optical devices incorporating single-mode optical fibers have been developed. R. Brown notably showed that the use of single-mode fibers and couplers would make it possible to carry out both homodyne and heterodyne DLS experiments.[4] An optical fiber-based interferometer has also been used to measure velocity profiles in sheared complex fluids, but not to determine velocities of nanometric-sized objects.[23,24] In addition, a couple of other teams have successfully performed heterodyne measurements using a fiber-optic sensor tip (optode) with a perpendicular exit face where the reflected light acts as local oscillator. Such reflected light was mixed in the fiber with the back scattered light from the sample (scattering angle fixed at 180°) to study diffusion in concentrated dispersions.[6,7,14] However, these setups do not allow a variation of the scattering angle and even less a control of the intensity level of the reference signal, I_{LO}. Thus, to the best of our knowledge, there is currently no user-friendly method for determining the speed and direction of a nano-object.

At the same time, emerging research is being developed today, particularly on complex active systems, texturing of new nanomaterials, and even cargo transport of particles. New experimental strategies must, however, be deployed to probe these new systems at nanoscales. In this context, HDLS could open up new perspectives, for example, in the field of active matter, which until now was limited to the study of micrometric-sized objects in 2D-confined environments. The study of the self-propulsion of active nanoparticles requires determining both the speed and direction of movement. This is possible here thanks to an original HDLS configuration involving optical fibers and integrated couplers, which offers both precise control of the LO signal and high sensitivity over the entire range of scattering vectors. Although the use of optical fibers facilitates the mixing of scattered and reference signals and greatly simplifies the implementation of such an HDLS experiment, it can introduce a phase shift between the two beams. These effects make autocorrelation functions more complex, which must, therefore, be established carefully.

The aim of this article is twofold: (i) we first detail in depth the heterodyne technique and the specific heterodyne correlation functions related to the use of optical fibers to mix the two interfering signals; (ii) the second part of the article successfully demonstrates the possibility of easily and accurately measuring the different relaxation modes associated with the dynamic processes of nano-objects in large statistical 3D ensembles. This type of measurement allows not only the study of motions of Brownian origin as in standard DLS but also a complete study of forced diffusion and propulsion processes. In particular, the motion of photocatalytic active AgCl nanoparticles with radius of ~70 nm that use electrolyte self-diffusiophoresis to achieve autonomous propulsion is fully characterized, allowing accurate determination of both random Brownian diffusion and ballistic contributions. Most importantly, their speed and propulsion directions are determined with great precision, pioneering results that demonstrate remarkable possibilities offered for future studies.

II. MATERIALS AND METHODS

A. Materials

Dispersions of silica nanoparticles (SiNPs) with radius R = 40 nm at a concentration of 2 wt. % were obtained by dilution of the required quantity of a commercial dispersion ([SiO_2] = 40.5 wt. %, pH = 9) of SNOWTEX ST-ZL colloidal silica from Nissan Chemical Industries, Ltd. (Tokyo, Japan). These colloidal silica dispersions are very stable in the 2–4 and 8–10 pH ranges and were used as received without further purification.

Suspension of small-sized photocatalytic silver chloride (AgCl) nanoparticles (NPs) (radius <100 nm) at a concentration of 4.9% was purchased from Thermo Scientific Chemicals. The stock solution was diluted 100 folds with dust-free deionized filtered water allowing to obtain stable 0.049% AgCl suspensions, thanks to their small size. DLS gives an apparent hydrodynamic radius of $R_{H,app} \geq 65$ nm. The analysis with the cumulant method also highlights a fairly polydisperse solution, indicating that individual NPs can form minority pairs or trinomials. The precise size of AgCl NPs was obtained using small-angle x-ray scattering (SAXS on beamline SWING at synchrotron Soleil, Saint-Aubin, France). A hard sphere model for the form factor gave a total radius equal to R = 72 nm, with a log-normal dispersion of σ = 0.165. A fresh 2 ml solution was prepared and transferred into a 1 cm diameter cylindrical scattering cell for each scattering angle measurement. To illuminate and activate the autonomous propulsion of the NPs, we use a 2 W/cm^2 irradiance UV LED source working at 365 nm from UWAVE.

Dispersion of 65 nm PSS NPs in water at a concentration of 0.2 g/l was also measured for comparison with the other systems studied.

A 20 μM–0.2% (in terms of tetramers) concanavaline A was prepared in a 0.05M HEPES buffer at pH = 6.9 also containing 0.15M NaCl, 0.001M $CaCl_2$, and 0.001M $MnCl_2$. Solutions were filtered through a 0.2 μm cellulose membrane.

B. Optical fiber heterodyne DLS setup

The measurements used a 3D light scattering spectrometer (LS Instruments, Fribourg, Switzerland) equipped with a 120 mW single transverse mode laser module (Ondax laser diode with typical linewidth of 300 MHz) operating at λ_0 = 638 nm and coupled to a single mode fiber (with a 4 μm germanium doped core fused with a 125 μm silica cladding, OZ Optics Ltd., Canada), a two-channel multiple tau correlator (1088 channels in autocorrelation), a variable-angle detection system mounted on a motorized goniometer (allowing the scattering angle to be varied between 15° and 150°), and a temperature-controlled index matching vat (LS Instruments). The scattering spectrum was measured using a single-mode fiber detection and a high sensitivity avalanche photodiode (APD) detector (Excelitas Technologies Canada, model SPCM-AQR-13-FC). Only one scattered beam of the 3D DLS setup was used to perform the experiments. All the components mentioned above, along with the optical bench and lenses, are arranged on an optical table forming an open and accessible setup.

The geometry of the configuration for the optic fiber heterodyne dynamic light scattering (HDLS) is shown in Fig. 2. This HDLS setup was implemented by modifying and updating the existing standard DLS configuration with the customized technical support

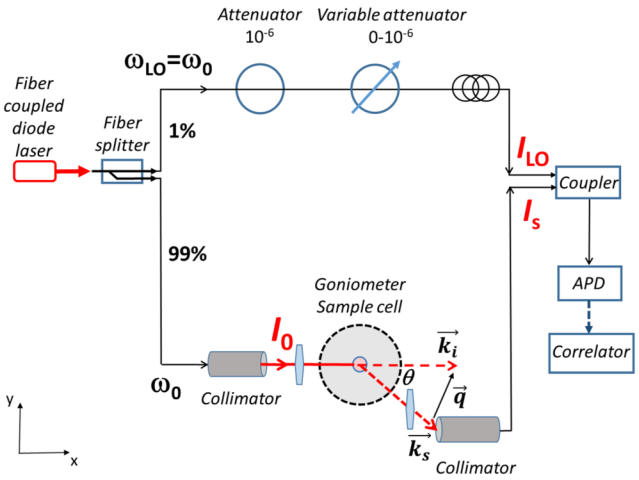

FIG. 2. Schematic of the optical fiber heterodyne DLS setup. The scattering angle θ can be varied between 15° and 150°.

from the company LS Instruments. HDLS experiments are possible here thanks to the mixing of interfering beams within a single-mode optical fiber specially designed for this project and manufactured on demand by OZ Optics Ltd. Specific mechano-optical mounts from LSI were used to integrate and align the fiber in the optical setup and to couple it directly to the monochromatic fiber laser. The resulting assembly is, therefore, unique and original, allowing easy switching from a standard homodyne configuration to a heterodyne configuration.

The specific optical fiber consists of a fiber-integrated fused beam splitter that operates by the splitting off of 1% of the laser light into a first arm that is used to carry the reference signal (local oscillator, LO), with the remaining 99% being directed into a second arm fiber and a lens-ended collimator with a focal length of 3.9 mm. 99% of the light (bottom of the scheme), which can be attenuated at the output of the collimator depending on the scattering level of the sample, constitutes the incident signal, I_0, and is subsequently directed through an optical lens (focal distance of 25 mm) to form a ~100 to 200 μm diameter beam waist in the middle of the sample scattering cell. Scattered light from the nanoparticle suspensions to be measured is collected by another optical lens (focal distance of 25 mm) and by another collimator (focal length of 3.9 mm) identical to the one used for the incident beam. The 1% signal (top of the scheme) is directed toward two successive optical attenuators, one having a fixed attenuation (10^{-6}) and the other allowing the LO signal to be varied (between 0 and 10^{-6}) and defined. This LO signal, I_{LO}, is directed into a fiber-integrated fused coupler made to meet up with the scattering signal, $I_s(\theta)$. In such a single-mode fiber-optic setup, a fiber coupler is then used instead of a beam splitter; the mode matching is then guaranteed without a special alignment. The single-mode fiber improves spatial coherence; it propagates only one transverse mode, maintains a phase correlation, and, at the output, the beams have a well-defined wavefront. As the same source is used for the scattering and reference signals, $\omega_{LO} = \omega_0$ (note that this case is similar to that used to describe the self-homodyne method in the optical communication literature).

The mixed signal is finally transported by the single-mode optical fiber to the avalanche single-photon-counting module (APD), with dark-count rate lower than 100 Hz, and processed by the correlator. The standard homodyne configuration is simply obtained by tacking $I_{LO} = 0$.

The distance between the laser output and the sample cell is only 0.84 m, while the path length of the LO reference signal (i.e., the branch separating the beam splitter and the coupler positioned before the photodiode) is about 3.6 m. It must be emphasized that such a length of fiber is necessary to connect the two successive attenuators and join the coupler and the photodiode arranged at the end of the goniometer arm without bending tension, particularly during its rotational motion. The optical path difference, L_{OPD}, is, therefore, of the order of 2.5 m, which results in a time difference $\tau_0 = \frac{L_{OPD}}{c/n}$ between the LO and the scattered signal of ~6×10^{-9} s, where c is the speed of light in vacuum and $n = 1.4$ is the refractive index in the fiber. These values are to be compared with the coherence length, $L_c = \frac{c}{n}\tau_{coherence}$, and coherence time, $\tau_{coherence} = \frac{1}{2\pi\Delta f}$, which directly depend on the laser characteristics. Based on the value of the linewidth of the diode laser equal to $\Delta f = 300$ MHz, it is estimated that $L_c = 0.1$ m and $\tau_{coherence} = 5.3 \times 10^{-10}$ s, which are values reflecting a regime $\tau_0 > \tau_c$ for which the phases of the interfering fields on the photodiode are uncorrelated.

C. Electric field and intensity correlation functions in homodyne DLS

The scattering vector is given by

$$\vec{q} = \vec{k_i} - \vec{k_s}\ , \quad q = \frac{4\pi n}{\lambda_0}\sin\frac{\theta}{2}, \tag{1}$$

where $\vec{k_i}$ and $\vec{k_s}$ are wave-vectors of the incident and scattered light, respectively. $\lambda_0 = 638$ nm is the incident wavelength at the laser; n the refractive index of the solvent ($n = 1.33$ at T = 20 °C for water); and θ is the scattering angle.

The scattered electric field at the detector is determined by the actual positions of the N scattering centers $\vec{r_m}(t)$ present in the scattering volume V.

$$E_s(q,t) = \sum_{m=1}^{N} A_m e^{i\vec{q}\vec{r_m}(t)} E_0 e^{-i[\omega_0 t + \phi_0(t)]}$$

$$= f(t) E_0 e^{-i[\omega_0 t + \phi_0(t)]}, \tag{2}$$

where A_m contains the amplitude factors for the mth particle, such as polarizability and the distance to the detector. ω_0 is the laser frequency; ϕ_0 is the phase shift; and $f(t) = \sum_{m=1}^{N} A_m e^{i\vec{q}\vec{r_m}(t)}$ is the modulation produced by the scattering process. If one assumes that all A_m values are identical, this latter quantity is proportional to $C(\vec{q},t) \equiv \sum_{m=1}^{N} e^{i\vec{q}\vec{r_m}(t)}$, which is the Fourier transform of the particle concentration $C(\vec{r},t)$ calculated over the scattering volume V. The relationship between the mean intensity averaged over the oscillation period (i.e., cycle average) and the field is defined as $I = (c\varepsilon_0/2)|E|^2$, where c is the velocity of light and ε_0 is the vacuum permittivity.[10,11,20] Since we are concerned with the relative intensity, the factor $c\varepsilon_0/2$ has been suppressed in the following sections. Therefore, the scattered intensity can be written as follows:

$$I_s(q,t) = E_s E_s^* = |f(t)|^2 E_0^2 = \sum_{m=1}^{N}\sum_{n=1}^{N} A_m A_n^* e^{i\vec{q}[\vec{r_m}(t) - \vec{r_n}(t)]} E_0^2, \tag{3}$$

where the subscript s refers to scattering. When the mutual positions of the scattering particles $r_m(t)$ change, the field E_s and the intensity I_s change accordingly. Hence, time correlations in the slow-changing (compared to the light frequency) $E_s(t)$ and $I_s(t)$ functions carry information about the particle motions.

The time dependence of $E_s(t)$ is characterized through the first-order time autocorrelation function of the scattered electric field,

$$G_s^{(1)}(q,\ \tau) \equiv \left\langle E_s^*(q,t) E_s(q,\ t+\tau)\right\rangle = \left\langle E_s^*(q,0) E_s(q,\ \tau)\right\rangle, \tag{4}$$

where τ is the delay time. The right-hand side of Eq. (4) represents the time average of the product of the complex conjugate of the field at time t with the field at time τ later. Assuming that $E_s(t)$ is a stationary random variable with properties that are independent of the time origin, t can be replaced with zero in Eq. (4). In accordance with the proportionality relationship $E_s(q,t) \propto C(\vec{q},t)$, the function $G_s^{(1)}$ (also called the heterodyne correlation function) is proportional to the coherent intermediate scattering function $F_1(\vec{q},\tau)$, or equivalently, to the autocorrelation function of concentration fluctuations,

$$G_s^{(1)} \propto F_1(\vec{q},\tau) \equiv \left\langle C^*(\vec{q},0) C(\vec{q},\tau)\right\rangle = \left\langle \sum_m \sum_n \exp\left(i\vec{q}\left[\vec{r_m}(\tau) - \vec{r_n}(0)\right]\right)\right\rangle. \tag{5}$$

It can be directly measured with the so-called heterodyne DLS. The quantity measured at the detector is the scattered intensity $I_s(t)$ rather than $E_s(t)$, and the second-order function $G_s^{(2)}$, which is often called the homodyne correlation function, is directly measured by the correlator connected to the APD light detector of the DLS setup,

$$G_s^{(2)}(q,\tau) = \langle I_s(q,t) I_s(q,t+\tau)\rangle = \langle I_s(q,0) I_s(q,\tau)\rangle. \tag{6}$$

For ergodic systems, the time averages in Eqs. (4)–(6) are equivalent to statistical averages over a long enough measuring time, t_{DLS}. In practice, the DLS experiments are often described using the normalized heterodyne and homodyne correlation functions,

$$g_s^{(1)}(q,\tau) = \frac{G_s^{(1)}(q,\ \tau)}{G_s^{(1)}(q,\ 0)} = \frac{\left\langle E_s^*(q,0) E_s(q,\ \tau)\right\rangle}{\langle I_s\rangle}$$

$$\propto \frac{F_1(q,\tau)}{F_1(q,0)} = \frac{\left\langle C^*(q,0) C(q,\tau)\right\rangle}{\left\langle C(q,0)^2\right\rangle}, \tag{7}$$

$$g_s^{(2)}(q,\tau) = \frac{G_s^{(2)}(q,\tau)}{G_s^{(2)}(q,\infty)} = \frac{\langle I_s(q,0) I_s(q,\tau)\rangle}{\langle I_s(q,0)\rangle^2}. \tag{8}$$

Hence, $g_s^{(1)}(q,0) = 1$ by definition. Note that $G_s^{(1)}(q,0) = \langle I_s(q,t)\rangle = I_s(q)$ gives the angular dependence of the time-averaged scattering intensity, where $I_s(q,t)$ is defined in Eq. (3). The limits of short and long times of the homodyne correlation function are

$g_s^{(2)}(q,0) = \frac{\langle I_s^2\rangle}{\langle I_s\rangle^2} = 2$ and $g_s^{(2)}(q,\infty) = \frac{\langle I_s\rangle^2}{\langle I_s\rangle^2} = 1$, respectively, so the function $g_s{}^{(2)}(q, \tau)$ decreases from 2 to 1. In general, $g_s{}^{(1)}(q, \tau)$ is not simply related to $g_s{}^{(2)}(q, \tau)$ in self-beat (*homodyne*) experiments. However, in special cases, such as in the so-called Gaussian approximation, the two DLS correlation functions are connected through the Siegert relation,

$$g_s^{(2)}(q,\tau) - 1 = \beta\left|g_s^{(1)}(q,\tau)\right|^2. \tag{9}$$

This relation expresses the fact that the electric field is made up of many statistically independent contributions, implying that E_s, which is itself a random variable, must be distributed according to a Gaussian distribution (an ideal case is a dilute solution of identical point-like particles). In Eq. (9), β is the so-called coherence factor, which depends on the optical geometry and samples; it is equal to 1 in ideal situation.

III. RESULTS AND DISCUSSION

A. Correlation functions in heterodyne optical fiber DLS

In the non-Gaussian case, the relation between $g_s{}^{(1)}(q, \tau)$ and $g_s{}^{(2)}(q, \tau)$ may contain extra useful information about the scattering processes. In addition, for complex dynamic processes of particles or molecules, such as forced diffusion exhibiting a velocimetry component in $g_s{}^{(1)}(q, \tau)$, an independent measurement of $g_s{}^{(1)}(q, \tau)$ is required. This may be accomplished by using the heterodyne technique, a method in which the scattered electric field is mixed with the reference light from a local oscillator source: here, the incident light from the same laser as that used for the scattering experiments.

The total electric field of the light at the detector is the sum of contributions from the local oscillator and light scattered from the sample. E_T can thus be expressed by a superposition of the scattered field E_s given by Eq. (2) with a frequency-shifted reference field E_L,

$$\begin{aligned} E_T(t) &= E_s(t) + E_L(t)e^{-i\Delta\omega t} \\ &= E_0\, f(t)e^{-i[\omega_0 t+\phi_0(t)]} + E_{LO}e^{-i[\omega_0 t+\phi_{LO}(t)]} \times e^{-i\Delta\omega t}, \end{aligned} \tag{10}$$

where the subscripts 0 and *LO* refer to the scattering and reference sources, respectively. $\Delta\omega = \omega_{LO} - \omega_0$ is the mean frequency difference between the two mixed fields; it is equal to 0 if the same source is used to generate both signals. Finally, $\phi(t)$ represents the total phase of the signal in each branch and may also contain the contribution associated with phase noise (see the Appendix). The measured count-rate heterodyne auto-correlation function is then given by

$$G_{het}^{(2)}(q,\tau) = \left\langle E_T^*(t)E_T(t)E_T^*(t+\tau)E_T(t+\tau)\right\rangle. \tag{11}$$

We must, however, distinguish two cases, depending on whether $\Delta\omega$ is zero or not.

1. Heterodyne correlation function in the $\Delta\omega \neq 0$ detection case

$G^{(2)}{}_{\text{het}}(q, \tau)$ is obtained by substituting Eq. (10) in Eq. (11) with $\Delta\omega \neq 0$. The expansion of Eq. (11) yields 16 terms, 10 of which, involving explicit time dependence appearing in the form of $\langle e^{\pm i\Delta\omega t}\rangle$, average out to zero. In addition, in practice, an HDLS experiment directly measures the normalized time heterodyne autocorrelation function, $g_{het}^{(2)} = \frac{G_{het}^{(2)}}{\langle I_{tot}\rangle^2}$, where $\langle I_{\text{tot}}\rangle^2 = \langle I_{\text{LO}}\rangle^2 + \langle I_s\rangle^2 + 2\langle I_{\text{LO}}\rangle\langle I_s\rangle$ is the square of the average total intensity measured at the detector, I_{LO} is the intensity of the reference beam, and $\langle I_s\rangle = \langle|f(t)|^2E_0{}^2\rangle$ is the time averaged scattered intensity. Using such normalization after a straight-forward calculation on the remaining terms allows us to obtain the following relationship:

$$\begin{aligned} g_{het}^{(2)} - 1 = \frac{\langle I_s\rangle^2}{\langle I_{tot}\rangle^2}\left(g_s^{(2)} - 1\right) + \frac{\langle I_{LO}\rangle\langle I_s\rangle}{\langle I_{tot}\rangle^2} \\ \times\left[\left\langle\frac{f^*(t)f(t+\tau)}{\langle|f(t)|^2\rangle}e^{i[\Delta\phi(t+\tau)-\Delta\phi(t)]}\times e^{i\Delta\omega\tau}\right\rangle + cc\right], \end{aligned} \tag{12}$$

where *cc* denotes the complex conjugate and $\Delta\phi(t)$ is the phase difference between the two interfering beams,

$$\Delta\phi(t) = \phi_{LO}(t) - \phi_0(t). \tag{13}$$

2. Heterodyne correlation function in the $\Delta\omega = 0$ detection case

Substituting Eq. (10) in Eq. (11) now gives rise to 16 terms, which are non-zero when $e^{\pm i\Delta\omega t} = 1$. The 10 additional terms compared to the previous case reflect the coupling of the two fields. It is important here to clarify the difference between implementations that use optical fibers and those that do not. If the LO and scattered fields originate from the same source, their phases are correlated as long as the optical path difference is less than the coherence length of the laser. The two fields are, therefore, spatially coherent through their common source and consequently statistically dependent even if their relevant dynamic (Brownian) fluctuations are independent. However, the use, for example, of a needle, which is necessarily rough and has nanometric aspirations, or of a scratch on the test tube to generate the reference signal (LO) causes random phase variations. The correlation with the incident field is lost and the two fields are, therefore, statistically independent. In the case where an optical fiber is used, this phase correlation is maintained and the fields remain statistically dependent. In the present case involving optical fibers with $\Delta\omega = 0$, correlation function (11) can be multiplied out and simplified to express $g_{\text{het}}{}^{(2)}$ as a function of $\Delta\phi(t + \tau)$ and $\Delta\phi(t)$ and their linear combinations,

$$g_{het}^{(2)}(q,\tau) - 1 = \begin{cases} \dfrac{\langle I_s\rangle^2}{\langle I_{tot}\rangle^2}\left[g_s^{(2)}(q,\tau) - 1\right] \\ + \dfrac{\langle E_0E_{LO}\rangle}{\langle I_{tot}\rangle}\left\langle f(t+\tau)e^{i\Delta\phi(t+\tau)} + f(t)e^{i\Delta\phi(t)}\right\rangle + cc \\ + \dfrac{\langle I_{LO}\rangle\langle I_s\rangle}{\langle I_{tot}\rangle^2}\left\langle\dfrac{f(t)f(t+\tau)}{\langle|f(t)|^2\rangle}e^{i[\Delta\phi(t+\tau)+\Delta\phi(t)]}\right\rangle + cc \\ + 2\dfrac{\langle I_{LO}\rangle\langle I_s\rangle}{\langle I_{tot}\rangle^2}\Re\left\langle\dfrac{f^*(t)f(t+\tau)}{\langle|f(t)|^2\rangle}e^{i[\Delta\phi(t+\tau)-\Delta\phi(t)]}\right\rangle, \end{cases} \tag{14}$$

where $\Re$ denotes the real part of the dynamical structure factor appearing in the fourth term. Equation (14) reveals two additional terms and their conjugates (second and third lines) compared to

the previous case ($\Delta\omega \neq 0$). A more complete calculation taking into account phase noise is given in the Appendix.

Importantly, $\Delta\phi(t)$ is the phase difference between the two interfering fields (originating from the same source here), which depends on the difference in the optical path taken by the two beams of the interferometer. In the coherent regime, the phases of the fields in the two branches are correlated with a constant mean phase difference of $\omega_0\tau_0$.[25–29] However, if this optical path difference (L_{OPD}) is greater than the distance over which the phases remain correlated, or equivalently when delay-time τ_0 is larger than the coherence time of the laser $\tau_{coherence} = \frac{1}{2\pi\Delta f}$, then $\Delta\phi$ is a function of lag-time τ. This is the case here with values for $L_{OPD} \sim 2.5$ m and $\tau_0 = 6 \times 10^{-9}$ s (see Sec. II), respectively, higher than those of the coherence length $L_c = 0.1$ m and $\tau_{coherence} = 5.3 \times 10^{-10}$ s, which directly depend on the characteristics of the laser. A consequence of this phase decorrelation is that the second and third terms of Eq. (14) will become oscillatory functions, i.e., depending on $\cos\Delta\phi(t+\tau)$ and $\cos[\Delta\phi(t) + \Delta\phi(t+\tau)]$, respectively. Their period is independent of the wave vector q, as observed in Fig. 3 showing the heterodyne correlation function $g_{het}^{(2)}(q, \tau)$ measured at various scattering angles between 30° and 130° for a SiNPs dilute solution with a 40 nm diameter . We can note that in certain cases (not shown), we observe two series of oscillations of different amplitude that are shifted from each other {cf. $\cos\Delta\phi(t+\tau)$ compared with $\cos[\Delta\phi(t) + \Delta\phi(t+\tau)]$ in second and third terms, respectively}. Note that the difference $\Delta\phi(t+\tau) - \Delta\phi(t)$ appearing in the fourth term of Eq. (14) should only moderately influence the structure factor $\frac{\langle f^*(t) f(t+\tau)\rangle}{\langle |f(t)|^2\rangle}$ generally visible in much higher lag-time regimes.

Therefore, the heterodyne intensity–intensity correlation function, $g_{het}^{(2)}(q, \tau)$, is oscillatory, showing more than 20 q-independent periods of $T = 1.8 \times 10^{-6}$ s. They are identical and observed for all study samples, such as SiNPs, AgCl NPS, polymeric NPs, and

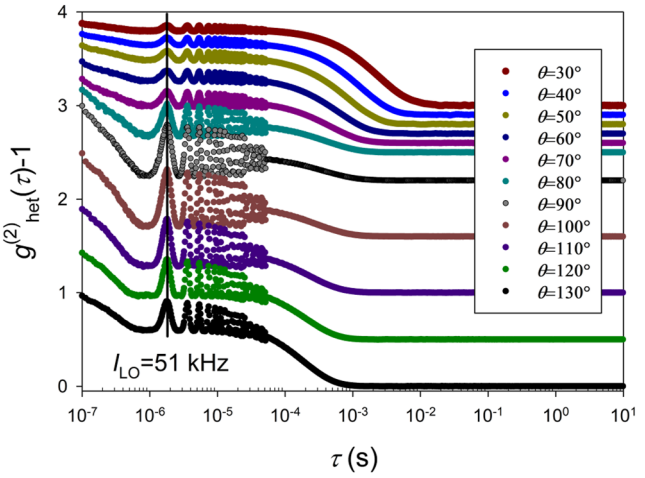

FIG. 3. Angular dependence of the heterodyne correlation function $g_{het}^{(2)}(q, \tau)$-1 recorded at various scattering angles, θ, for a $c = 2$ wt. % 40 nm SiNPs solution. For the sake of clarity, curves are shifted vertically. The dashed line represents the θ-independent position of the first oscillation. The intensity of the reference signal $I_{LO} = 51$ kHz is kept constant here for all scattering angles.

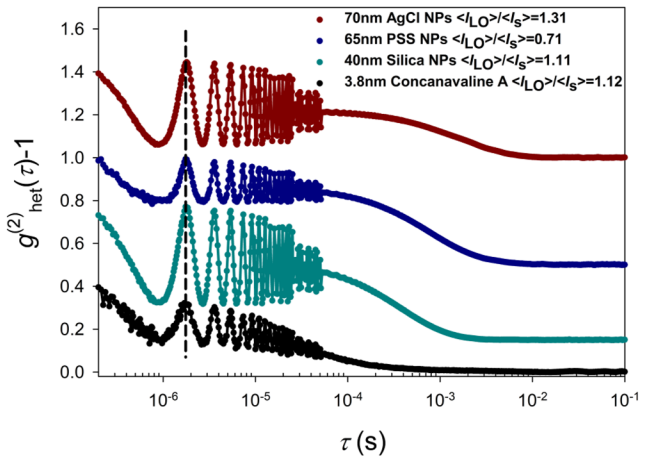

FIG. 4. Heterodyne DLS correlation function $g_{het}^{(2)}(q, \tau) - 1$ measured at $\theta = 90°$ for a 40 nm SiNPs solution at $c = 2$ wt. %, a 70 nm AgCl NPs solution at 0.049 wt. %, a 65 nm PSS polymeric NPs solution at 0.2 g/l, and a 3.8 nm radius concanavaline A dilute solution at 2.02 g/l. The curves are shifted vertically to improve visibility. The $\langle I_{LO}\rangle/\langle I_s\rangle$ ratios are close to 1 and, therefore, correspond to the maximum possible heterodyne contribution $A_{heterodyne} = 2\langle I_{LO}\rangle\langle I_s\rangle/\langle I_{tot}\rangle^2 = 0.5$.

proteins (see Fig. 4). In order to clearly visualize these short-time range oscillations, their amplitude was maximized by choosing an appropriate value for the LO intensity. The exponential decay observed at longer time scales is associated with the Brownian diffusive relaxation of the particles (see net Sec. III B).

It is appropriate here to recall and summarize the different possible expressions that the heterodyne intensity autocorrelation function, $g_{het}^{(2)}$, can take, depending on the experimental configuration. Even though in all cases, $g_{het}^{(2)}$ contains the term that depends on $\Re\left[g_s^{(1)}\right]$ $\left(\text{equivalently } \Re\left[\frac{\langle f^*(t) f(t+\tau)\rangle}{\langle f^2(t)\rangle}\right]\right)$ and, therefore, the information associated with the dynamics of the sample, its expression may differ depending on whether the two beams originate from the same source and whether the arrangement uses optical fibers or not.

(i) In the case where an HDLS experiment is performed without the use of optical fibers, using, for example, the reflection of the incident laser by a solid object immersed in the sample (e.g., a needle) as a reference signal, the scattered and LO fields are considered to be statistically independent, which implies that $\langle E_{LO}(t)E_s(t)\rangle = \langle E_{LO}(t)\rangle\langle E_s(t)\rangle$. In addition to the fact that the two fields originate from distinct physical processes, this stems from their phase difference being random. This is the case if they come from different sources (e.g., $\Delta\omega \neq 0$), but more generally, the different portions of the field reflected, for example, by a needle that has irregularities on the optical scale or by a scratch, undergo random phases in all cases. It can be noted that the mixing of the fields took place at a photomultiplier during these early experiments. In this case, the mathematical expansion of $g_{het}^{(2)}$ reveals several zero terms, those involving $\langle E(t)E(t+\tau)\rangle$ or those linear in E (the same applies to complex conjugates), which gives a fairly simple

expression similar to Eq. (12) and corresponds to the known expression in the literature.[10,11] If we take advantage of the random nature of the phases, ϕ_0 and ϕ_{LO}, the term in Eq. (12) containing $\Delta\phi$ vanishes. In the case where the same source is used for the scattered and local oscillator beams ($\Delta\omega = 0$), $\Delta\phi$ is related to the difference in path taken by the two beams but becomes random due to the arbitrary reflections mentioned above. Even though the expression of $g_{het}^{(2)}$ is much simpler, the realization of this type of experiment is, as discussed previously, far too complicated, with major drawbacks, such as the lack of control of the LO signal and a limited angular variation linked to random reflections of the immersed solid or the scratch introduced on the surface of the sample tube.

(ii) In the more user-friendly case where a fiber optic setup is used, two cases must be considered: If $\Delta\omega \neq 0$, the expression for $g_{het}^{(2)}$ remains simple and is given by Eq. (12). This is related, as calculated above, to the fact that 10 terms are zero because $\langle e^{\pm i\Delta\omega t}\rangle = 0$. However, such an experiment would prove too complex to carry out with the integration of two different sources operating at two different wavelengths. An assembly using optical fibers and a single source facilitates routine measurements but introduces several coupling terms, which do not cancel out when $\Delta\omega = 0$. The expansion of Eq. (11) thus gives 16 terms, all non-zero because the fields are not statistically independent (the phase correlation between the two fields is not lost) and because the term $\langle e^{\pm i\Delta\omega t}\rangle$ no longer appears in the equations. Such considerations have been described in the field of optical communications using the superposition of a laser field and a time-delayed image of itself, notably to measure the linewidth of the laser.[25–29] However, no study reports an expression of $g_{het}^{(2)}$ involving a field scattered by a sample in optical fibers and which is a function of its response factor $f(t)$ and its autocorrelation. It was, therefore, necessary to detail its expression given by Eq. (14), which will be essential for future studies involving HDLS.

Although such coupling effects, which depend on the phase shift between the two fields (i.e., on the OPD), must be taken into account when performing optic-fiber HDLS, they are not troublesome and only visible for very short lag-time regimes lying outside the time window of the correlator associated with the dynamic relaxation modes (i.e., $g_s^{(1)}$) of the systems studied. However, measuring their amplitude proves useful because it allows, as Sec. III A 3 shows, for the LO signal level to be correctly dosed.

Thus, for larger lag time regimes related to dynamic processes of interest, such as nanoparticle diffusion and propulsion, the second and third terms of Eq. (14) can be neglected and the correlation function can be approximated as follows:

$$g_{het}^{(2)} - 1 \approx \frac{\langle I_s\rangle^2}{\langle I_{tot}\rangle^2}\left(g_s^{(2)} - 1\right) + 2\frac{\langle I_{LO}\rangle\langle I_s\rangle}{\langle I_{tot}\rangle^2}\Re\left\langle g_s^{(1)} \times e^{i[\omega_0\tau+\phi_{LO}(t+\tau)-\phi_{LO}(t)]}\right\rangle. \tag{15}$$

In order to obtain this equation, which is simply the addition of a homodyne term depending on $g_s^{(2)}$ and a heterodyne term, we introduced the scattered electric field correlation function $g_s{}^{(1)}(q,\tau)$ defined previously by Eq. (7). Its expression in terms of $f(t)$ is given by the following relation:

$$g_s^{(1)}(q,\tau) = \frac{\langle E_s^*(q,t)E_s(t+\tau)\rangle}{\langle I_s\rangle} = \left\langle \frac{f^*(t)f(t+\tau)}{\langle|f(t)|^2\rangle} e^{-i[\omega_0\tau+\phi_0(t+\tau)-\phi_0(t)]}\right\rangle. \tag{16}$$

The correlation functions of Eqs. (12) and (15) differ only in the extra $e^{i\Delta\omega\tau}$-factor entering the heterodyne formula for $\Delta\omega \neq 0$.

3. Effect of the variation in intensity of the local oscillator

Importantly, the heterodyne contribution [second term of the right-hand side of Eq. (15)] allowing determination of the real part of the dynamical structure factor (i.e., autocorrelation function of concentration fluctuations) is proportional to the product of the scattered intensity and reference beam, $\langle I_s\rangle\langle I_{LO}\rangle$, and can be easily modulated using the variable attenuator. Note that since the ratio between the contributions of the self-beating (homodyne) term, $g_s{}^{(2)}$, and the heterodyne term, $\Re[g_s{}^{(1)}]$, is proportional to $\langle I_s\rangle/2\langle I_{LO}\rangle$, Eq. (15) can be reduced to the second heterodyne term if the added reference signal dominates the scattering signal: $\langle I_{LO}\rangle \gg \langle I_s\rangle$. Some authors have noticed that the signal-to-noise ratio could be increased by an increase in the reference signal to dominate the detector noise.[9,30] However, the modern APD used in this study has a very low noise, which is less than 1 kHz and much smaller than the experimental signal. Furthermore, several considerations must be taken into account when increasing I_{LO}. The homodyne amplitude, $A_{homodyne} = \langle I_s\rangle^2/\langle I_{tot}\rangle^2$, decreases continuously with I_{LO}, while the heterodyne amplitude passes through a maximum, $A_{heterodyne} = 2\langle I_{LO}\rangle\langle I_s\rangle/\langle I_{tot}\rangle^2 = 0.5$, obtained for $\langle I_{LO}\rangle/\langle I_s\rangle = 1$. Concomitantly, the intercept of the correlation function $g_{het}^{(2)}(0) - 1 = A_{Homodyne} + A_{Heterodyne}$ is, however, very reduced. Large I_{LO} implies a low intercept, and hence, the recovery of the dynamic information becomes less accurate. Thus, an optimal dosage of $\langle I_{LO}\rangle/\langle I_s\rangle$ must be defined in order to measure good quality correlograms and to avoid the intercept approaching zero and the amplitude of the dynamic relaxation modes being too close to the baseline. It is also often important to obtain simultaneous measurements of both homodyne and heterodyne contributions.[6,7] As seen in Fig. 5(a), the amplitude (equivalently the intercept) of the exponential relaxation visible for $\tau > 5 \times 10^{-5}$ s and which reflects the Brownian diffusion of 40 nm SiNPs is indeed considerably reduced when $\langle I_{LO}\rangle/\langle I_s\rangle$ is increased. The decrease in $g_{het}^{(2)}(0) - 1$ obtained after extrapolation to zero-τ for a $\langle I_{LO}\rangle/\langle I_s\rangle$ ratio varying from 0 to 3 is reported in Fig. 5(b) and displays a variation qualitatively in good agreement with that predicted theoretically and given by $\langle I_s\rangle^2/\langle I_{tot}\rangle^2 + 2\langle I_{LO}\rangle\langle I_s\rangle/\langle I_{tot}\rangle^2$. The shift between the theoretical and experimental curves observed in this figure is certainly due to the reduction in coherence factor β with I_{LO} as well as possibly due to the laser noise via the pre-factor $C(\tau,\tau_0)$ entering into Eqs. (A8) and (A9) (see the Appendix).

Finally, a prior measurement of the amplitude of the fast oscillations observed in the very short-time range of the correlation function, which is proportional to the injected LO level, probes to be an effective calibration method and a prerequisite for tuning the optimal $\langle I_{LO}\rangle/\langle I_s\rangle$ ratio and defining a sufficient heterodyne contribution while maintaining a suitable intercept for the particles relaxations modes.

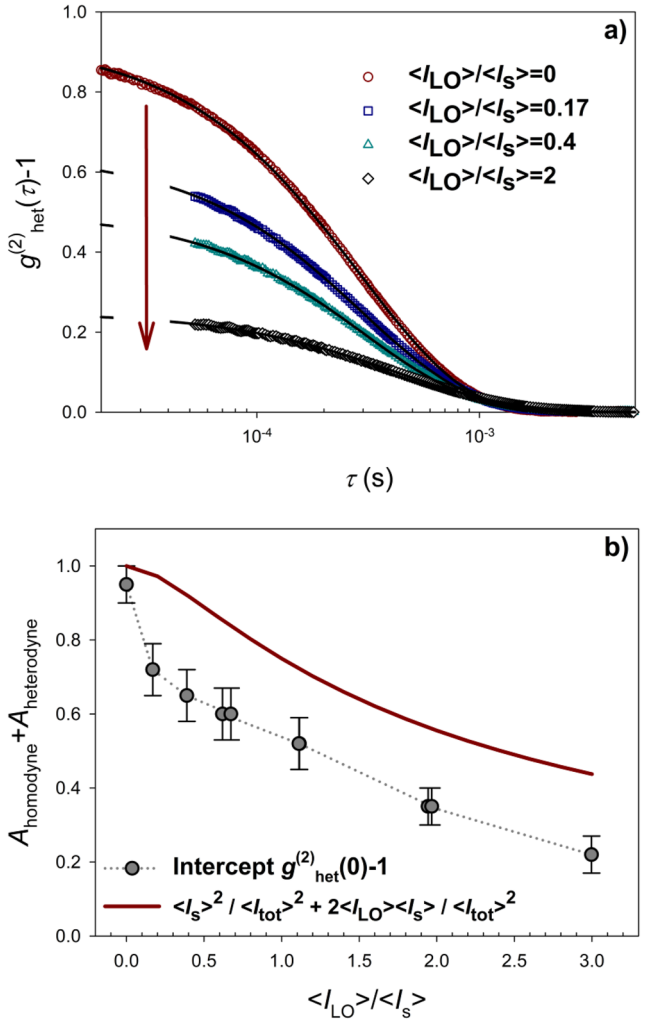

FIG. 5. Heterodyne intensity correlation function $g_{het}^{(2)}(q, \tau) - 1$ recorded at various $\langle I_{LO}\rangle/\langle I_s\rangle$ ratios at $\theta = 90°$ for a $c = 2$ wt. % 40 nm SiNPs solution (curves are not shifted and fast oscillations are cut for clarity) (a). Evolution of the intercept $g_{het}^{(2)}(0) - 1$ with $\langle I_{LO}\rangle/\langle I_s\rangle$ compared with the theoretical prediction (continuous line) (b).

B. Dilute solution of identical Brownian particles: Translational diffusion

If the scattering particles are identical and if the solution is dilute enough, we can assume their trajectories to be statistically independent and Eq. (5) simplifies to[10,11]

$$F_1(\vec{q},\tau) = \langle N\rangle\left\langle \exp\left(i\vec{q}\left[\vec{r_m}(\tau) - \vec{r_m}(0)\right]\right)\right\rangle = \langle N\rangle F_s(\vec{q},\tau). \quad (17)$$

The exponential factor reflects the statistical properties of the particle displacement $\Delta\vec{r_m}(\tau) = \vec{r_m}(\tau) - \vec{r_m}(0)$, which are expected to be the same for all particles in the scattering volume V. The summation has been dropped and the factor $\langle N\rangle$ inserted since each particle has the same statistical behavior. $\langle N\rangle \equiv \langle N(t)\rangle$ is the statistical average of the number of particles in V. $F_s(\vec{q},\tau)$ is the so-called self-intermediate scattering function which characterizes the displacement of a particle during lag-time τ,

$$F_s(\vec{q},\tau) = \left\langle e^{i\vec{q}\left[\vec{r_m}(t+\tau) - \vec{r_m}(t)\right]}\right\rangle. \quad (18)$$

For stationary systems, any joint point probability distribution does not change with a time shift t, so F_s depends on τ, but not on t. For $q \neq 0$, the boundary conditions are $F_s(\vec{q},0) = 1$ and $F_s(\vec{q},\infty) = 0$. With this quantity being identical for each particle m, the average scattered intensity $\langle I_s\rangle = N\langle|A_m|^2\rangle E_0^2$ and the field correlation function $G_s^{(1)}$ are found to be proportional to the product of single particle correlation functions. Therefore, the normalized function $g_s^{(1)}$ directly gives the self-intermediate scattering function $F_s(\vec{q},\tau)$ of the particles,

$$g_s^{(1)}(\vec{q},\tau) = \frac{G_s^{(1)}(\vec{q},\tau)}{\langle I_s\rangle} = F_s(\vec{q},\tau)\times e^{-i[\omega_0\tau + \phi_0(t+\tau) - \phi_0(t)]}, \quad (19)$$

which can be directly measured with heterodyne DLS,

$$g_{het}^{(2)} - 1 \approx \frac{\langle I_s\rangle^2}{\langle I_{tot}\rangle^2}\left(g_s^{(2)} - 1\right) + 2\frac{\langle I_{LO}\rangle\langle I_s\rangle}{\langle I_{tot}\rangle^2}\Re[F_s(q,\tau)]. \quad (20)$$

In the case of a solution of Brownian particles that do not interact directly with each other, F_s is a decreasing exponential,

$$F_s(\vec{q},\tau) = F_s(\vec{q},0)e^{-D_T q^2\tau} = e^{-D_T q^2\tau}, \quad (21)$$

where D_T is the translational diffusion coefficient of the particles, which allows their hydrodynamic radius R_H to be determined via the Stokes–Einstein relationship if the absolute temperature T and the viscosity of solvent η are known,

$$D_T = \frac{k_B T}{6\pi\eta R_H}. \quad (22)$$

Unlike the homodyne function $g_s^{(2)}$, the heterodyne function $g_{het}^{(2)}$ contains both $\left|g_s^{(1)}(\tau)\right|^2$ and $\Re[g_s^{(1)}(\tau)]$ (i.e., $\Re[F_s(\tau)]$) terms and is the superposition of two relaxations,

$$g_{het}^{(2)} - 1 = \frac{\langle I_s\rangle^2}{\langle I_{tot}\rangle^2}e^{-2D_T q^2\tau} + 2\frac{\langle I_{LO}\rangle\langle I_s\rangle}{\langle I_{tot}\rangle^2}e^{-D_T q^2\tau}, \quad (23)$$

where $g_s^{(2)} - 1 = \left|g_s^{(1)}\right|^2 = \exp\left(-2D_T q^2\tau\right)$. Equations (20)–(23) do not take into account the phase jitter $\Delta\phi(t,\tau)$, and for clarity, the very short time part ($\tau < 5\times10^{-5}$ s) of the correlation functions is cut in the following figures. $g_{het}^{(2)}$ was measured at different scattering angles θ for a dilute solution of 70 nm AgCl NPs with optimal $\langle I_{LO}\rangle/\langle I_s\rangle$ ratios between 1.5 and 2 in order to obtain well-defined relaxation modes with good amplitudes and intercepts (see Fig. 6). Fitting heterodyne correlation functions using Eq. (23) gives the decay time, $\tau_c = 1/D_T q^2$, which is inversely proportional to q^2. Such a variation is the signature of a pure Brownian diffusion process (see the inset of Fig. 6) and allows us to determine a value of 1.1×10^6 nm^2/s for D_T after extrapolation of $1/\tau_c q^2$ to zero-q. These results are naturally in perfect agreement with those obtained from self-beating experiments conducted with $I_{LO} = 0$, thereby validating the optical fiber based heterodyne DLS method.

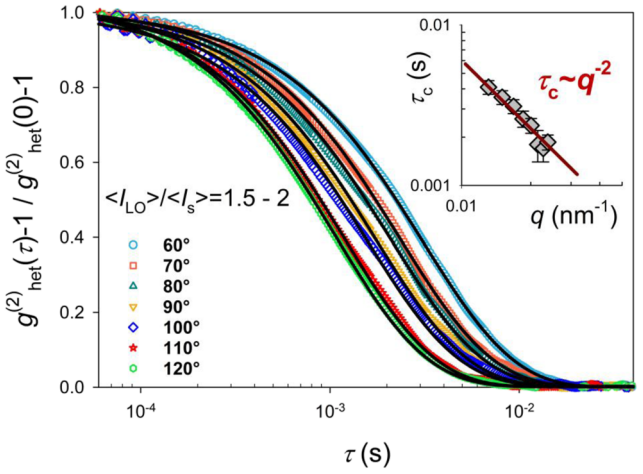

FIG. 6. Heterodyne intensity correlation function $g_{het}^{(2)}(q, \tau)$-1 recorded at various scattering angles, θ, for a $c = 0.049\%$ AgCl solution. The ratio $\langle I_{LO}\rangle/\langle I_s\rangle$ is varying between 1.5 and 2 depending on the scattering angle. Correlation functions are normalized by their values obtained at $\tau = 5 \times 10^{-5}$ s and well-fitted using Eq. (23) (see the continuous lines). The inset shows the variation of the decay time with q.

C. Identical particles subjected to directed propulsion

Let us now consider a dilute solution of identical diffusive scattering particles, which are forced to move with an average velocity $\vec{v}$ due to an external field (e.g., magnetic, electrostatic,[15,18,19] gravitational[31] etc.) or a macroscopic flow (e.g., convective flow[20,32,33]). In the particular case of active nanoparticles, autonomous directed propulsion can be created by an "engine" transforming an external source of energy into mechanical works.[22,34–38] In all these situations where particles exhibit both random translational diffusion and directed drift, the particle concentration $C(\vec{r}, t)$ satisfies the equations derived for a forced diffusion,

$$\frac{\partial C(\vec{r},t)}{\partial t} + \nabla \vec{J} = 0 \; ; \; \vec{J} = \vec{v} C(\vec{r},t) - D_T \nabla C(\vec{r},t), \qquad (24)$$

where $\vec{J}(\vec{r}, t)$ is the particle flux. Solving Eq. (24) gives the Green function $F_s(\vec{r}, t)$ (or equivalently the Van Hove correlation function), which is a conditional probability to find the particle at the point $\vec{r}$ at time t if initially it was at $\vec{r} = \vec{0}$,[10,11]:

$$F_s(\vec{r},t) = \frac{1}{(4\pi D_T t)^{d/2}} \exp\left(-\frac{(\vec{r} - \vec{v}\,t)^2}{4D_T t}\right), \qquad (25)$$

where d is the space dimension. Spatial Fourier transformation, subject to the appropriate boundary condition $F_s(\vec{q}, 0) = 1$, yields

$$F_s(\vec{q},\tau) = e^{i\vec{q}\,\vec{v}\,\tau} e^{-q^2 D_T \tau}. \qquad (26)$$

Diffusion and ballistic terms, which depend on D_T and $\vec{v}$, respectively, enter as independent factors. For the heterodyne experiment, Eq. (26) gives

$$g^{(2)}_{het} - 1 = \frac{\langle I_s\rangle^2}{\langle I_{tot}\rangle^2}\left(g_s^{(2)} - 1\right) + 2\frac{\langle I_{LO}\rangle\langle I_s\rangle}{\langle I_{tot}\rangle^2} \cos \vec{q}\,\vec{v}\,\tau \times e^{-D_T q^2 \tau}. \qquad (27)$$

The second term of $g_{het}^{(2)}(q, \tau)$ is oscillatory, but decays because of the damping exponential term. The frequency of these oscillations, $\omega = \vec{q}\,\vec{v}$, carries the information about the value and the direction of the velocity of the particles provided the scattering vector is varied. Therefore, beating between the two interfering fields preserves information on the velocity of the particles (responsible of the detected frequency shift $\vec{q}\,\vec{v}$ relative to ω_0) and is the basis of laser Doppler velocimetry.[13–19] The function $g_s^{(2)} \sim |F_s|^2 \sim \exp(-2D_T q^2 \tau)$ that is accessible using standard DLS only contains the diffusive information.

Active nanoparticles capable of autonomous directed propulsion are expected to play a central role in nanoscience and nanomedicine, with applications based on cargo transport to a specific location or on the texturing and functionalization of nanomaterial surfaces.[34–38] However, a decrease in size to the nanoscale presents new experimental challenges. First, nanopropellers become too small to be tracked using optical microscopy. Second, their dynamics and collective behaviors in large three-dimensional statistical ensembles constitute an unexplored area of study. Therefore, heterodyne optical fiber DLS turns out to be a new technique of choice for measuring the speed and direction of nanoparticles. In this context, UV-light activated spherical silver chloride nanoparticles (AgCl NPs) capable of producing autonomous directed propulsion by electrolyte self-diffusiophoresis are suitable candidates to validate our technical approach.[22,39–41] More precisely, a UV light irradiation induces the reduction of silver chloride to Ag at the surface of the particles and the release of H^+ and Cl^- ions with different diffusivities: the diffusion coefficient of small-size H^+ is $D_{H^+} = 9.311 \times 10^{-5}$ cm^2 s^{-1}, while that of Cl^- is only $D_{Cl^-} = 2.032 \times 10^{-5}$ cm^2 s^{-1},[39–41]

$$4\,AgCl + 2H_2O + h\nu \rightarrow 4\,Ag + 4H^+ + 4Cl^- + O_2. \qquad (28)$$

Due to the asymmetric photodecomposition of the particles, which is either due to particle surface heterogeneity or non-uniform UV-exposure of the particles, the surface reaction generates a local ionic concentration gradient and an endogenous net electric field, in response to which the nanoparticles move [Fig. 7(a)]. In this work, 0.049 wt. % solutions of AgCl NPs with radius $R \sim 70$ nm are illuminated by a focused UV beam oriented with an angle $\varphi_{UV} = 15°$ in the (xy) plane, where φ_{UV} is the angle between the incident laser beam and the UV irradiation [see Fig. 7(a)]. The UV LED source operating at 365 nm is positioned 6 cm from the center of the scattering cell resulting in an irradiance of 0.5 W/cm^2 and a beam diameter of 1.7 cm in the scattering volume. It should be noted that minimal UV absorption remains possible.

Remarkably, few seconds after the UV light was turned on, a very clearly defined series of damped oscillations appears in $g^{(2)}_{het}$ for delay times greater than 10^{-3} s and unambiguously reflects a propulsive process characterized by an average velocity [Fig. 7(b)]. In addition, a ratio $\langle I_{LO}\rangle/\langle I_s\rangle \sim 1.5$ was used so that the heterodyne relaxation amplitude associated with such propulsive process is maximal while maintaining a good quality intercept. The dependence of the oscillation frequency on the scattering wave-vector q_{xy} (or equivalently on the scattering angle θ) observed in Fig. 7(b) clearly indicates that propulsion occurs in the (xy) plane. Fitting correlation functions with Eq. (27) allows us to determine the

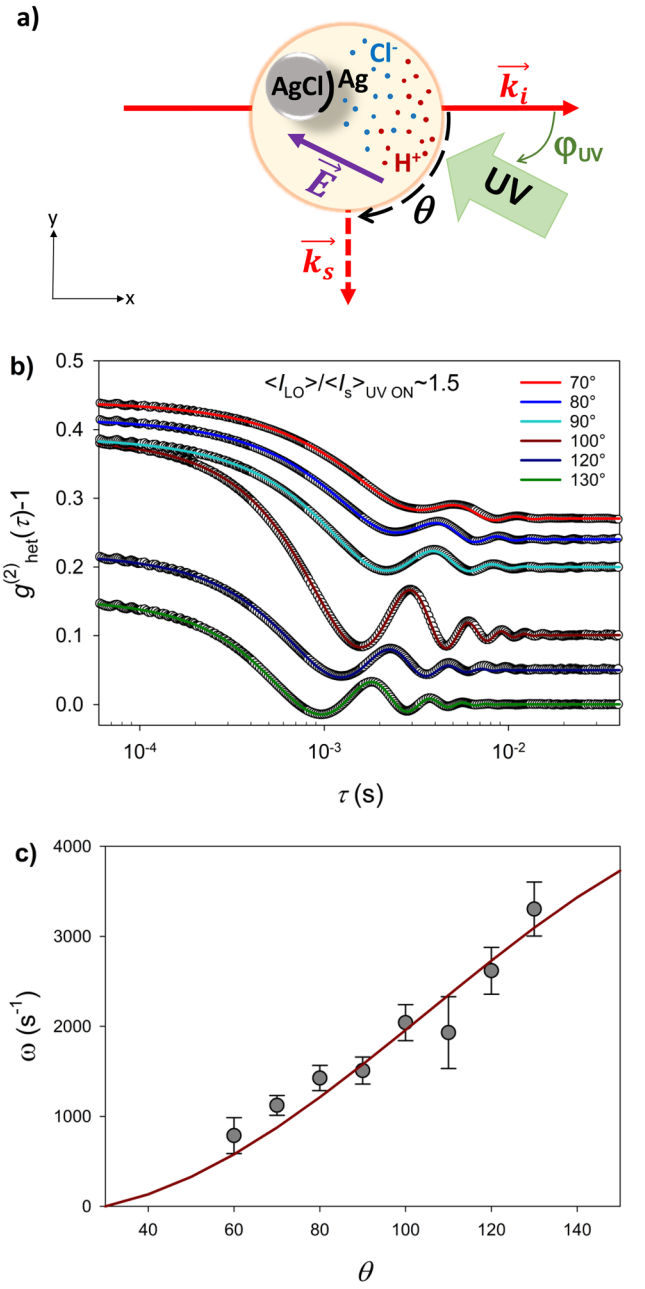

FIG. 7. Principle of the self-propelled motion of AgCl NPs by UV-induced electrolyte self-diffusiophoresis. The net electric field that powers the motion is due to the local ionic concentration gradient generated by the difference in diffusivity of the ionic species (a). Scattering angle θ dependence of $g_{het}^{(2)}(q, \tau) - 1$ (a fresh AgCl solution was prepared for each angle measurement) for a UV beam orientation $\varphi_{UV} = 15°$, an irradiance of 0.5 W/cm^2, and 500 s after the UV illumination was switched on. Continuous lines represent the best fits of the data using Eq. (27). The curves are vertically shifted to improve the visibility. The very short-time range oscillations due to the phase shift between the interfering signals and appearing for $\tau < 5 \times 10^{-5}$ s have been masked here (b). The frequency dependence on θ and its best fit can be visualized in Fig. 7(c).

q-dependent frequency ω. Its variation reported in Fig. 7(c) gives speed v and its direction,

$$\omega = \vec{q}\,\vec{v} = \vec{k}_i\,\vec{v} - \vec{k}_s\,\vec{v} = \frac{2\pi n}{\lambda} v[\cos\alpha - \cos(\theta - \alpha)], \qquad (29)$$

where α is the direction angle between $\vec{k}_i$ and $\vec{v}$. One obtains an impressive speed of $v = 170\ \mu\text{m s}^{-1}$ and a direction of $\alpha \sim \varphi_{UV} + k\pi$, showing that the trajectory of the propulsion is imposed by the orientation of the UV irradiation. It is important to remember here that active nanoparticles are also subject to rotational diffusion and F_s will, therefore, depend not only on D_T and v but also on the rotational diffusion coefficient D_R.[34–36] For particles that are optically anisotropic (polarizability of AgCl NPs is not homogeneous under UV irradiation), the exponential decay depends on both D_T and D_R.[10,11,22] D_R was estimated to be equal to 19.2 rad^2 s^{-1} with a characteristic rotation time τ_R of 52 ms.[22] The long-time scale regime $\tau \gg \tau_R$ for which rotational diffusion leads to a randomization of the direction of propulsion corresponds to the long-time scale baseline of the correlation function and is, therefore, not visible in our DLS experiments. In addition, the persistence length over which NPs move in the direction of their original orientation $L = v/D_R$ is around few micrometers and is larger than the scattering length scale $1/q$. In the time and length scales accessible in DLS, the motion of active NPs is, therefore, well-described by a forced diffusion process. Despite their small size and low Reynolds number, such active NPs have impressive speeds, which agree with the Helmholtz–Smoluchowski equation: $v = \varepsilon\zeta E/\eta$. Here, E represents the electric field generated by the local ionic gradient and scales with the surface reaction rate that is to say with the UV irradiance.[35,39–41] For a given zeta potential ζ, the velocity is maximized by the directed UV exposure, in response to which particles (with $\zeta < 0$) travel toward its direction.

IV. CONCLUSION

In summary, the use of optical fibers makes it easier to carry out of heterodyne dynamic light scattering experiments, provides great versatility, but also generates a contribution to the heterodyne intensity correlation function at very short time scales, which may depend on the difference in the optical path taken by the scattered and LO interfering signals and on the linewidth of the laser. These instrumental effects, however, appear in a time domain very far from that associated with dynamic particle processes and above all make it possible to optimize the experimental conditions by weighting the heterodyne contribution best suited to the system.

Heterodyne dynamic light scattering proves to be a method of first choice to study the dynamic processes of nanometric particles capable of producing self-propulsion or being subjected to external fields. It also allows easily and directly determining the direction and speed of complex objects of various natures (colloids, nanoparticles, polymers, and proteins) that are too small to be followed by optical microscopy. Finally, such an optical approach should open up new perspectives not only in the study of active matter but also in various fields related to nanotechnology and biotechnology.

ACKNOWLEDGMENTS

This work was supported by the Agence Nationale pour la Recherche (Grant Nos. MONA_LISA ANR-20-CE09-0012 and PHOTOMORPH ANR-24-CE06-7386, fellowship to A.C.). The authors thank A. Vaccaro (LSI, Freiburg, Switzerland) and acknowledge the Université Paris Cité (France).

AUTHOR DECLARATIONS

Conflict of Interest

The authors have no conflicts to disclose.

Author Contributions

Anastasia Christoulaki: Formal analysis (equal); Investigation (equal); Writing – review & editing (equal). **Eric Buhler**: Conceptualization (lead); Formal analysis (equal); Funding acquisition (lead); Investigation (equal); Supervision (lead); Validation (equal); Writing – review & editing (lead).

DATA AVAILABILITY

The data that support the findings of this study are available within the article.

APPENDIX: DETAILED DERIVATION OF THE CORRELATION FUNCTION

The total electric field E_T at the detector is given by

$$E_T(t) = E_s(t) + E_{LO}(t) = E_0 f(t) e^{-i[\omega_0 t + \phi_0(t)]} + E_{LO} e^{-i[\omega_0 t + \phi_{LO}(t)]} \times e^{-i\Delta\omega t}, \tag{A1}$$

where $\Delta\omega = \omega_{\mathrm{LO}} - \omega_0$ is the frequency difference between the local oscillator LO and the incident light. $\phi(t)$ is the total phase of the signal in each branch, which, as detailed later, also contains the contribution associated with phase noise. Finally, the amplitudes of the fields, E_0 and E_{LO}, are assumed to be constant in time. The heterodyne beat signal is thus given by the following expression:

$$I_{het}(t) = |E_T|^2 = E_{LO}^2 + |f(t)|^2 E_0^2 + E_{LO} E_0 f(t) e^{i[\phi_{LO}(t) - \phi_0(t) + \Delta\omega t]} + cc, \tag{A2}$$

where cc denotes the complex conjugate of the preceding term. The auto-correlation function for I_{het} (second-order correlation function) is

$$G_{het}^{(2)}(q,\tau) = \langle I_{het}(q,t) I_{het}(q,\ t+\tau)\rangle = \left\langle E_T^*(t) E_T(t) E_T^*(t+\tau) E_T(t+\tau)\right\rangle. \tag{A3}$$

1. Case for which $\Delta\omega \neq 0$:

The function $G^{(2)}{}_{\mathrm{het}}(q, \tau)$ can be multiplied out and simplified to obtain

$$G_{het}^{(2)}(q,\tau) = \left\langle I_{LO}^2\right\rangle + 2\langle I_{LO}\rangle\langle I_s\rangle + \left\langle E_0^2\right\rangle^2 \left\langle |f(t)|^2 |f(t+\tau)|^2\right\rangle + \left\langle E_0^2 E_{LO}^2 f^*(t) f(t+\tau) e^{i[\phi_{LO}(t+\tau) - \phi_0(t+\tau) - \phi_{LO}(t) + \phi_0(t)]} \times e^{i\Delta\omega\tau}\right\rangle + cc, \tag{A4}$$

where we have used the following result: $\left\langle e^{\pm i\Delta\omega t}\right\rangle = \langle \cos \Delta\omega t\rangle + i\langle \sin \Delta\omega t\rangle = 0$, which reduces the total number of terms to six instead of 16. I_{LO} is the intensity of the local oscillator and $\langle I_s\rangle = \langle |f(t)|^2 E_0{}^2\rangle$ is the time averaged scattered intensity by the sample. In practice, the HDLS experiments are described using the normalized time autocorrelation functions, $g_{het}^{(2)} = \frac{G_{het}^{(2)}}{\langle I_{tot}\rangle^2}$ and $g_s^{(2)}$, where the total intensity measured at the detector is given by $\langle I_{\mathrm{tot}}\rangle^2 = \langle I_{\mathrm{LO}}\rangle^2 + \langle I_s\rangle^2 + 2\langle I_{\mathrm{LO}}\rangle\langle I_s\rangle$,

$$g_{het}^{(2)} - 1 = \frac{\langle I_s\rangle^2}{\langle I_{tot}\rangle^2}\left(g_s^{(2)} - 1\right) + \frac{\langle I_{LO}\rangle\langle I_s\rangle}{\langle I_{tot}\rangle^2} + \left[\left\langle \frac{f^*(t) f(t+\tau)}{\langle |f(t)|^2\rangle} e^{i[\Delta\phi(t+\tau) - \Delta\phi(t)]} \times e^{i\Delta\omega\tau}\right\rangle + cc\right], \tag{A5}$$

where $\Delta\phi(t) = \phi_{LO}(t) - \phi_0(t)$ denotes the phase difference between the two interfering beams.

2. Case for which $\Delta\omega = 0$:

In this paragraph, we perform an analysis quite similar to that of the previous one, with the difference that $\left\langle e^{\pm i\Delta\omega t}\right\rangle = 1$. Consequently, there are ten additional terms compared to the previous case that depend on the coupling between the two fields, which are considered statistically dependent when using optical fibers. We reiterate that both fields originate from the same source. It can be pointed out that this case is similar to that used to describe the self-homodyne method in the optical communication literature for statistically dependent interfering fields,[25–29]

$$g_{het}^{(2)}(q,\tau) - 1 = \begin{cases} \frac{\langle I_s\rangle^2}{\langle I_{tot}\rangle^2}\left[g_s^{(2)}(q,\tau) - 1\right] \\ + \frac{\langle E_0 E_{LO}\rangle}{\langle I_{tot}\rangle}\left\langle f(t+\tau) e^{i\Delta\phi(t+\tau)} + f(t) e^{i\Delta\phi(t)}\right\rangle + cc \\ + \frac{\langle I_{LO}\rangle\langle I_s\rangle}{\langle I_{tot}\rangle^2}\left\langle \frac{f(t) f(t+\tau)}{\langle |f(t)|^2\rangle} e^{i[\Delta\phi(t+\tau) + \Delta\phi(t)]}\right\rangle + cc \\ + \frac{\langle I_{LO}\rangle\langle I_s\rangle}{\langle I_{tot}\rangle^2}\left\langle \frac{f^*(t) f(t+\tau)}{\langle |f(t)|^2\rangle} e^{i[\Delta\phi(t+\tau) - \Delta\phi(t)]}\right\rangle + cc. \end{cases} \tag{A6}$$

Although this result is sufficient to interpret the correlation functions, one can go further by decoupling the total phase into two contributions, one associated with the signal in each branch and the other with the phase noise of the laser: $\phi(t) = \varphi_{sign}(t) + \varphi_n(t)$, where φ_{sign} is φ_0 or φ_{LO} depending on the branch of the interferometer. The noise $\varphi_n(t)$ is a stochastic process representing the random phase fluctuation, which leads to the broadening of the spectral line. We could also include a fixed phase difference φ' due to the interferometer's couplers/beam splitters. The phase noise jitter $\Delta\varphi_n(t,\tau) = \varphi_n(t+\tau) - \varphi_n(t)$, i.e., the random phase change between times t and $t+\tau$, is usually assumed to be a Gaussian noise with zero-mean. Its variance increases linearly with time delay τ, $\left\langle \Delta\varphi_n(t,\tau)^2\right\rangle = \left\langle \Delta\varphi_n(\tau)^2\right\rangle = 2\pi\Delta f|\tau|$, where $2\pi\Delta f$ is the angular full linewidth at half maximum of the Lorentzian optical profile line.[25–28] Since the scattered signal and the LO are seeded from the same source, their phase noise can be assumed to be shifted by a time-delay of τ_0 due to the optical path difference between the two branches of the setup, namely, $\varphi_n(t) \equiv \varphi_{LO,\ n}(t) = \varphi_{0,\ n}(t+\tau_0)$. τ_0 also refers to the possible remaining phase correlation between the two combined beams. This is the optical time delay for unbalanced

interferometric systems or the dispersion time for the polarization-dispersed modes in single mode fiber mixing.[25] Therefore, by using the well-known relationship for Gaussian random variables,

$$\left\langle e^{\left[\pm i\Delta\varphi_n(t,\tau)\right]}\right\rangle = e^{\left[-\frac{1}{2}\left\langle\Delta\varphi_n(\tau)^2\right\rangle\right]}. \tag{A7}$$

$g_{het}^{(2)}$ can be expressed as a function of $\left\langle\Delta\varphi_n(\tau)^2\right\rangle$ and $\left\langle\Delta\varphi_n(\tau_0)^2\right\rangle$,

$$g_{het}^{(2)}(q,\tau)-1 = \begin{cases} \dfrac{\langle I_s\rangle^2}{\langle I_{tot}\rangle^2}\left[g_s^{(2)}(q,\tau)-1\right] \\ +\dfrac{\langle E_0E_{LO}\rangle}{\langle I_{tot}\rangle}\left\langle f(t)e^{i\Theta(t)}+f(t+\tau)e^{i\Theta(t+\tau)}\right\rangle \times e^{A(\tau_0)}+cc \\ +\dfrac{\langle I_{LO}\rangle\langle I_s\rangle}{\langle I_{tot}\rangle^2}\left\langle\dfrac{f(t)f(t+\tau)}{\langle|f(t)|^2\rangle}\times e^{i[\Theta(t)+\Theta(t+\tau)]}\right\rangle \times e^{B(\tau,\tau_0)}+cc \\ +2\dfrac{\langle I_{LO}\rangle\langle I_s\rangle}{\langle I_{tot}\rangle^2}\Re\left\langle\dfrac{f^*(t)f(t+\tau)}{\langle|f(t)|^2\rangle}\times e^{i[\Theta(t+\tau)-\Theta(t)]}\right\rangle \times e^{C(\tau,\tau_0)}, \end{cases} \tag{A8}$$

where

$$\begin{cases} A(\tau_0) = -\dfrac{1}{2}\left\langle\Delta\varphi_n{}^2(\tau_0)\right\rangle, \\ B(\tau,\tau_0) = \left\langle\Delta\varphi_n{}^2(\tau)\right\rangle - \left\langle\Delta\varphi_n{}^2(\tau_0)\right\rangle - \dfrac{\left\langle\Delta\varphi_n{}^2(\tau+\tau_0)\right\rangle}{2} - \dfrac{\left\langle\Delta\varphi_n{}^2(\tau-\tau_0)\right\rangle}{2}, \\ C(\tau,\tau_0) = -\left\langle\Delta\varphi_n{}^2(\tau)\right\rangle - \left\langle\Delta\varphi_n{}^2(\tau_0)\right\rangle + \dfrac{\left\langle\Delta\varphi_n{}^2(\tau+\tau_0)\right\rangle}{2} + \dfrac{\left\langle\Delta\varphi_n{}^2(\tau-\tau_0)\right\rangle}{2}, \end{cases} \tag{A9}$$

and $\Re$ denotes the real part of the complex correlation function [dynamical structure factor appearing in the fourth term of Eq. (A8)]. To obtain this result, it was assumed that $\Delta\varphi_n$ and $\varphi_{LO}(t)-\varphi_0(t)$ were independent. Phase noise occurs in the form of pre-factors and could contribute to a decrease in the amplitude of the correlation function. Importantly, $\Theta(t)=\varphi_{LO}(t)-\varphi_0(t)$ is the phase difference between the two signals, which depends on the difference in optical paths taken by the two beams of the interferometer (see the main text).

REFERENCES

[1] J. M. Hogan and M. A. Kasevich, "Atom-interferometric gravitational-wave detection using heterodyne laser links," Phys. Rev. A **94**, 033632 (2016).
[2] K. S. Thorne, "Gravitational-wave research: Current status and future prospects," Rev. Mod. Phys. **52**, 285 (1980).
[3] G. J. Verbiest and M. J. Rost, "Beating beats mixing in heterodyne detection schemes," Nat. Commun. **6**, 6444 (2015).
[4] R. G. W. Brown, "Homodyne optical fiber dynamic light scattering," Appl. Opt. **40**, 4004 (2001).
[5] J. B. Salmon, S. Manneville, A. Colin, and B. Pouligny, "An optical fiber based interferometer to measure velocity profiles in sheared complex fluids," Eur. Phys. J.: Appl. Phys **22**, 143 (2003).
[6] D. Lilge and D. Horn, "Diffusion in concentrated dispersions: A study with fiber-optic quasi-elastic light scattering (FOQELS)," Colloid Polym. Sci. **269**, 704–712 (1991).
[7] L. G. B. Bremer, L. Deriemaeker, R. Finsy, E. Geladé, and J. G. H. Joosten, "Fiber optic dynamic light scattering, neither homodyne nor heterodyne," Langmuir **9**, 2008–2014 (1993).
[8] H. Z. Cummins and E. R. Pike, *Photon Correlation Spectroscopy and Velocimetry* (Plenum Press, New York, 1977).
[9] E. Jakeman, "Photon correlation," in *Photon Correlation and Light Beating Spectroscopy*, edited by H. Z. Cummins and E. R. Pike (Plenum Press, New York, 1974), pp. 75–149.
[10] B. J. Berne and R. Pecora, *Dynamic Light Scattering with Applications to Chemistry, Biology, and Physics* (Dover Publications, INC, Mineola, NY, 2000).
[11] C. S. Johnson, Jr. and D. A. Gabriel, *Laser Light Scattering* (Dover Publications, Inc., New York, 1981).
[12] B. Chu, *Laser Light Scattering, Basic Principles and Practice* (Dover Publications, Inc., Mineola, NY, 2007).
[13] T. Tanaka, C. Riva, and I. Ben-Sira, "Blood velocity measurements in human retinal vessels," Science **186**, 830 (1974).
[14] T. Tanaka and G. B. Benedek, "Measurement of the velocity of blood flow (in vivo) using a fiber optic catheter and optical mixing spectroscopy," Appl. Opt. **14**, 189 (1975).
[15] B. R. Ware, "Electrophoretic light scattering," Adv. Colloid Interface Sci. **4**, 1 (1974).
[16] N. Ben-Yosef, S. Zweigenbaum, and A. Weitz, "Mass motion as observed by light-beating spectroscopy," Appl. Phys. Lett. **21**, 436 (1972).
[17] R. V. Mustacich and B. R. Ware, "Observation of protoplasmic streaming by laser-light scattering," Phys. Rev. Lett. **33**, 617 (1974).
[18] B. R. Ware and W. H. Flygare, "The simultaneous measurement of the electrophoretic mobility and diffusion coefficient in bovine serum albumin solutions by light scattering," Chem. Phys. Lett. **12**, 81 (1971).
[19] B. R. Ware and W. H. Flygare, "Light scattering in mixtures of BSA, BSA dimers, and fibrinogen under the influence of electric fields," J. Colloid Interface Sci. **39**, 670 (1972).
[20] E. Moulin, I. A. Nyrkova, N. Giuseppone, A. N. Semenov, and E. Buhler, "Homodyne dynamic light scattering in supramolecular polymer solutions: Anomalous oscillations in intensity correlation function," Soft Matter **16**, 2971 (2020).
[21] N. Jouault, E. Moulin, N. Giuseppone, and E. Buhler, "Light scattering strategy for the investigation of time-evolving heterogenous supramolecular self-assemblies," Phys. Rev. Lett. **115**, 085501 (2015).
[22] A. Christoulaki and E. Buhler, "Light-induced directed self-propulsion of active nanosized particles in a three-dimensional Brownian environment probed by heterodyne photon correlation laser spectroscopy," Phys. Rev. E **111**, 015433 (2025).
[23] J. B. Salmon, S. Manneville, and A. Colin, "Shear banding in a lyotropic lamellar phase. I. Time-averaged velocity profiles," Phys. Rev. E **68**, 051503 (2003).
[24] J. B. Salmon, S. Manneville, and A. Colin, "Shear banding in a lyotropic lamellar phase. II. Temporal fluctuations," Phys. Rev. E **68**, 051504 (2003).
[25] P. Gallion and G. Debarge, "Quantum phase noise and field correlation in single frequency semiconductor laser systems," IEEE J. Quantum Electron. **20**, 343–349 (1984).
[26] P. Gallion, F. J. Mendieta, and R. Leconte, "Single-frequency laser phase-noise limitation in single-mode optical-fiber coherent-detection systems with correlated fields," J. Opt. Soc. Am. **72**, 1167–1170 (1982).
[27] H. Ludvigsen, M. Tossavainen, and M. Kaivola, "Laser linewidth measurements using self-homodyne detection with short delay," Opt. Commun. **155**, 180–186 (1998).
[28] I. Attia, E. Wohlgemuth, O. Balciano, R. J. Cohen, Y. Yoffe, and D. Sadot, "Laser linewidth characterization via self-homodyne measurement under nearly-coherent conditions," Opt. Express **30**, 14492–14504 (2022).
[29] T. Okoshi, K. Kikuchi, and A. Nakayama, "Novel method for high resolution measurement of laser output spectrum," Electron. Lett. **16**, 630–631 (1980).
[30] C. J. Olivier, "Correlation techniques," in *Photon Correlation and Light Beating Spectroscopy*, edited by H. Z. Cummins and E. R. Pike (Plenum Press, New York, 1974), pp. 151–223.
[31] A. Wada, I. Nishio, and K. Soda, "Rapid investigation of sedimentation phenomena by vibrational force field," Rev. Sci. Instrum. **50**, 458 (1979).
[32] A. Sehgal and T. A. P. Seery, "Anomalous dynamic light scattering from solutions of light absorbing polymers," Macromolecules **32**, 7807–7814 (1999).
[33] W. Schaertl and C. Roos, "Convection and thermodiffusion of colloidal gold tracers by laser light scattering," Phys. Rev. E **60**, 2020 (1999).
[34] J. R. Howse, R. A. L. Jones, A. J. Ryan, T. Gough, R. Vafabakhsh, and R. Golestanian, "Self-motile colloidal particles: From directed propulsion to random walk," Phys. Rev. Lett. **99**, 048102 (2007).
[35] J. L. Moran and J. D. Posner, "Phoretic self-propulsion," Annu. Rev. Fluid. Mech. **49**, 511 (2017).

[36]C. Bechinger, R. Di Leonardo, H. Löwen, C. Reichhardt, G. Volpe, and G. Volpe, "Active particles in complex and crowded environments," Rev. Mod. Phys. **88**, 045006 (2016).
[37]A. Ghosh and P. Fischer, "Controlled propulsion of artificial magnetic nanostructured propellers," Nano Lett. **9**, 2243 (2009).
[38]S. J. Ebbens, "Active colloids: Progress and challenges towards realising autonomous applications," Curr. Opin. Colloid Interface Sci. **21**, 14 (2016).
[39]P. Illien, R. Golestanian, and A. Sen, "Fuelled' motion: Phoretic motility and collective behaviour of active colloids," Chem. Soc. Rev. **46**, 5508 (2017).
[40]M. E. Ibele, P. E. Lammert, V. H. Crespi, and A. Sen, "Emergent, collective oscillations of self-mobile particles and patterned surfaces under redox conditions," ACS Nano **4**, 4845 (2010).
[41]M. Ibele, T. E. Mallouk, and A. Sen, "Schooling behavior of light-powered autonomous micromotors in water," Angew. Chem., Int. Ed. **48**, 3308 (2009).